Optical Materials 68 (2017) 11–18

Contents lists available at ScienceDirect

Optical Materials

journal homepage: www.elsevier.com/locate/optmat

Direct inkjet printing of miniaturized luminescent YAG:Er^{3+} from sol-gel precursor

Yuzhe Hong [a], Zhaoxi Chen [a], Artem A. Trofimov [a, c], Jincheng Lei [b, c], Jie Chen [d], Lei Yuan [b, c], Wenge Zhu [b, c], Hai Xiao [b, c], Dong Xu [a, e], Luiz G. Jacobsohn [a, c], Konstantin G. Kornev [a], Rajendra K. Bordia [a], Fei Peng [a, c, *]

[a] Department of Materials Science and Engineering, Clemson University, Clemson, SC 29634, USA
[b] Department of Electrical and Computer Engineering, Clemson University, Clemson, SC 29634, USA
[c] COMSET - Center for Optical Materials Science and Engineering Technologies, Clemson University, Anderson, SC 29635, USA
[d] School of Physics and Electrical Technology, Yancheng Teachers University, Yancheng, Jiangsu 224002, China
[e] School of Material Science and Engineering, Jiangsu University, No. 301 Xuefu Road, Zhenjiang 212013, PR China

ARTICLE INFO

Article history:
Received 30 September 2016
Received in revised form
8 December 2016
Accepted 12 December 2016
Available online 23 December 2016

Keywords:
Direct inkjet printing
Sol-gel
YAG
Scintillator

ABSTRACT

This work focuses on demonstrating the fabrication of miniaturized scintillators based on rare earth activated YAG ceramics using the direct inkjet printing method. Erbium was chosen as the activator, and YAG sol-gel precursor inks were prepared under precise hydrolysis and polycondensation reactions. The precursors showed excellent control over rheology and surface tension, resulting in good printability. One of the most important challenges of inkjet printing of lines is the stability of lines. Line stability during printing is highly dependent on the printing frequency, drop spacing and substrate temperature. When a line was printed drop by drop, bulges were always observed during printing at 25 °C. This instability was significantly suppressed when the substrates were slightly heated. Adding polyvinylpyrrolidone to the precursor helped eliminate pores and cracks during firing. Crack-free YAG lines with ~200 nm thickness were obtained after firing. The photoluminescence of YAG:Er heat-treated at 1200 °C for 1 h was optimized for an Er concentration of 2 wt%. X-ray induced radioluminescence was dominated by emission lines at 398 and 567 nm.

1. Introduction

Polycrystalline ceramic and single-crystal scintillators are widely used in medical imaging, security inspection and high energy physics [1–3]. In many applications, the scintillator needs to be fabricated into specific geometries, *e.g.*, sheets [4] and fibers [5], to allow the optimal performance or to satisfy specific needs. For example, fiber scintillators have been used to measure the particle radiation dose for local cancer treatment [5]. Thus, it is highly desired to be able to fabricate miniaturized ceramic scintillators into complex geometries for specific applications, or as a part of integrated smart devices. However, due to the high hardness and brittleness of ceramics, they are difficult to fabricate into complex shapes in small dimensions (*e.g.* smaller than 100 μm) using the traditional bulk sintering and machining method [6].

Direct inkjet printing is a promising method to fabricate complex ceramic features because the ceramic precursors can be directly deposited at specific positions with high spacial resolution [7]. Many ceramic systems have been directly printed on substrates using the inkjet printing method [8–14]. Some complex parts, such as ZrO_2 mazes [8] and Si_3N_4 gear wheels [14], have been successfully fabricated using this method. However, commonly used inks are made of dispersed nanopowders in a liquid medium [8–10]. Besides the challenge of dispersion, the ceramic nanoparticles tend to concentrate at the edge of the drop during drying. This effect is known as the 'coffee ring' effect [15] and it results in uneven depositions of ceramic powder on the substrates. One can avoid the coffee ring effect by using a ceramic sol-gel precursor instead of a nanopowder dispersion as the ink for direct inkjet printing. Ceramic sol-gel precursors allow one to uniformly mix the solute molecules [16] thus avoiding concentration gradients in the printed drops. However, there are no systematic studies of the stability of the printed lines formed by the sol-gel inks. In addition, post processing and sintering efficiency of the printed sol-

* Corresponding author. Department of Materials Science and Engineering, Clemson University, Clemson, SC 29634, USA.

http://dx.doi.org/10.1016/j.optmat.2016.12.020
0925-3467/

Table 1
The compositions of inks.

Ink	YW	YWP	YWEP
YAG yield	2.5%	2.5%	2.5%
Solvent	DI water	DI water	DI Water: ethanol = 7:1 by weight
PVP addition	No	Yes	Yes

gel lines have not been studied.

In this work, we aimed at demonstrating the use of direct inkjet printing to fabricate miniaturized rare earth activated YAG-based scintillators. Toward this goal, we used sol-gel derived YAG:Er^{3+} precursor to create lines of ~100 μm width. To obtain stable lines without bulges, we studied the effect of drop spacing, substrate moving speed and substrate temperature. Finally, the luminescence of sintered YAG:Er^{3+} was characterized by means of photo- and radioluminescence measurements.

2. Experimental procedure

The YAG precursor was prepared from aluminum isopropoxide (AIP, $Al(C_3H_7O)_3$, 98%, Alfa Aesar, MA, USA), aluminum nitrate nonahydrate (AN, $Al(NO_3)_3{\cdot}9H_2O$, 98%, Alfa Aesar, MA, USA) and yttrium nitrate hexahydrate (YN, $Y(NO_3)_3{\cdot}6H_2O$, 99.9%, Alfa Aesar, MA). Erbium nitrate pentahydrate (EN, $Er(NO_3)_3{\cdot}5H_2O$, 99.9%, Sigma, MO) was used as the starting material of the activator, and deionized (DI) water was used as the solvent. The molar ratio of AIP: AN: YN: DI water was 3.5:1.5:3:100 in order to make stoichiometric YAG. AN and YN were first dissolved in deionized water at room temperature by vigorously stirring for 30 min. Then AIP was added into the solution and stirred for 20 h. The solution was then refluxed at 80 °C for 5 h. Approximately 2/3 of the solvent was removed using a rotary evaporator (IKA RV 10 digital, China). The resultant solution was dried in an oven at 80 °C until viscous sols were obtained. The hydrolyzed sols were diluted with DI water or water-ethanol mixture solution using an ultrasonic processor. The YAG yield w is defined as $= m/m_0 \times 100\%$, where m is the mass of product after firing at 1200 °C for 1 h and m_0 is the mass of the ink before firing. The YAG yield in the inks was diluted to 2.5%. Polyvinylpyrrolidone (PVP, M_w 58,000 Da, Sigma-Aldrich, MO, USA) was added to relax stresses during srying. The PVP weight to the YAG yield was set to be 30%. Three different inks were investigated: YAG sol in water (YW); YAG sol in water with PVP (YWP); and YAG sol in water and ethanol with PVP (YWEP). The compositions of the final inks are shown in Table 1.

Fused silica plates were used as substrates. To clean them, they were ultrasonicated in the following sequence: DI water, ethanol and acetone, each for 10 min. After sonication, substrates were dried in an oven. A piezo-electric drop-on-demand printhead (MJ-AT-01-40, orifice diameter 40 μm, MicroFab Inc., Plano, TX, USA) was used in this study. The diameter of the generated droplet was about 60 μm, as measured using a high speed camera. The printing frequency was set to 200 Hz. To study the effect of droplet spacing, p, on the printing stability, the moving speed of the substrate was set as: $v = pf$ for a given p, where f is the printing frequency. The

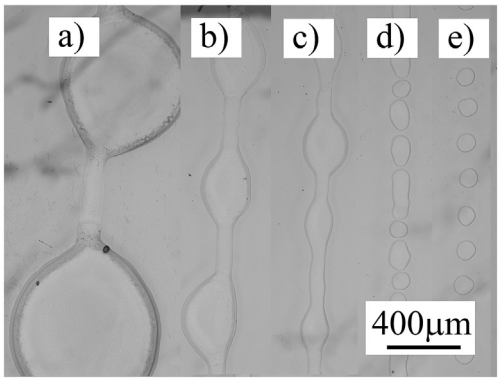

Fig. 1. Optical microscopy images of printed lines using YWP ink at room temperature with different drop spacing: a) 5 μm; b) 25 μm; c) 50 μm; d) 100 μm; d) 200 μm.

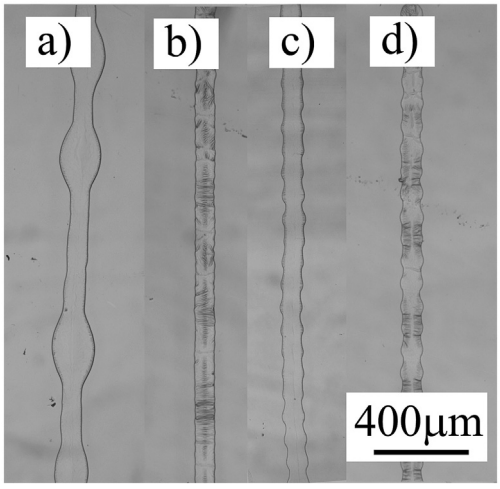

Fig. 2. Optical microscopy images of printed lines using YWP ink on heated substrates at different temperature and drop spacings: a) 57 °C, 50 μm; b) 95 °C, 50 μm; c) 76 °C, 100 μm; d) 95 °C, 100 μm.

viscosities of the inks were measured using an Ubbelohde viscometer (Cannon instrument, PA, USA) under water bath. The advancing and receding contact angles, and surface tension were measured using a Kruss drop shape analyzer (DSA100, Hamburg, Germany).

After printing, the samples were dried in an oven at 80 °C for 24 h and then fired at 1200 °C for 1 h with heating rate of 10 °C/min. Differential thermal analysis (DTA) and thermogravimetric analysis (TGA) of YAG gel were carried out using a DTA7 analyzer (Perkin Elmer, MA) and a TGA7 analyzer (Perkin Elmer, MA). In order to identify the phases using X-ray diffraction (XRD, Rigaku Co., Ltd., Tokyo, Japan), YAG powder was prepared from YAG gel by firing at a target temperature for 1 h. The fully-dried printed patterns were characterized using optical microscope (Olympus BX60). The microstructure of printed patterns after firing was characterized using scanning electron microscope (SEM, Hitachi S4800, Hitachi,

Table 2
The rheology data and Z values of the inks.

Ink	Density (g/cm^3)	Viscosity (10^{-3} Pa·s)	Surface tension (mN/m)	Z	Advancing contact angle (°)	Receding contact angle (°)
YW	1.04	1.09	61.72 ± 0.08	5.17	47 ± 1	19 ± 2
YWP	1.04	1.11	64.94 ± 0.08	5.10	45 ± 1	15 ± 2
YWEP	1.01	1.51	42.50 ± 0.05	3.23	37 ± 2	15 ± 2

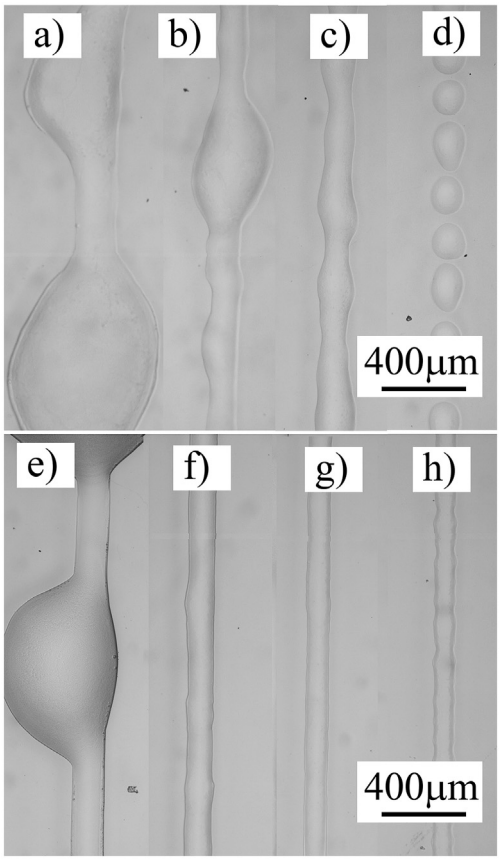

Fig. 3. Optical microscopy images of printed lines using YWEP ink at different substrate temperatures and drop spacings. Substrate temperature, a) – d): 25 °C; e) - h): 40 °C. Drop spacing: a) and e) = 5 μm; b) and f) = 25 μm; c) and g) = 50 μm; d) and h) = 100 μm.

Ltd., Tokyo, Japan). The widths of the printed tracks were observed from the top-view using the optical or electron microscopy. The thickness features of the printed patterns were measured using an Atomic Force Microscope (WITec Aplpha 300, WITec GmbH, Ulm, Germany).

Photoluminescence spectra were obtained using a Horiba Jobin Yvon Fluorolog 3 spectrofluorometer equipped with double monochromators for both excitation and detection, and a 450 W xenon lamp as the excitation source. All measurements were carried out in ambient conditions with excitation set at 381 nm and detection spectral resolution of 1 nm.

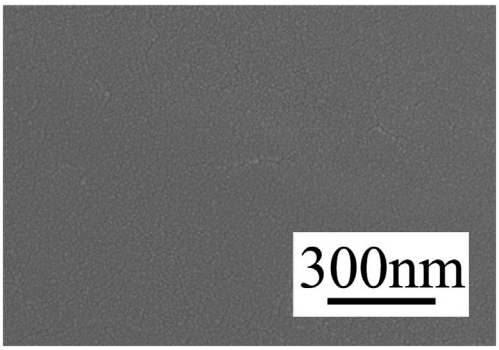

Fig. 5. SEM micrograph of a dried line printed using YWEP ink. Substrate temperature is 40 °C and drop spacing = 50 μm.

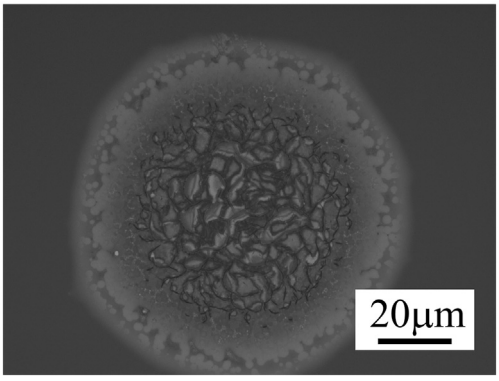

Fig. 6. Optical image of a printed drop using YW ink after firing at 1200 °C for 1 h.

Scintillation was evaluated by means of radioluminescence measurements under X-ray excitation using a custom-designed Lexsyg Research spectrofluorometer (Freiberg Instruments, Germany) equipped with a VF-50J X-ray tube (Varian Medical Systems, UT) with a W target and operated at 40 kV and 1 mA, and a DU920P-BU Newton CCD camera (Andor Technology, UK). Spectra were not corrected for the spectral sensitivity of the system.

3. Results and discussion

3.1. Ink printability

The density, viscosity, surface tension, and droplet formation parameter, *Z* of the sol-gel inks, are given in Table 2, where Z is the printability of the inks calculated using Eq (1) [15]:

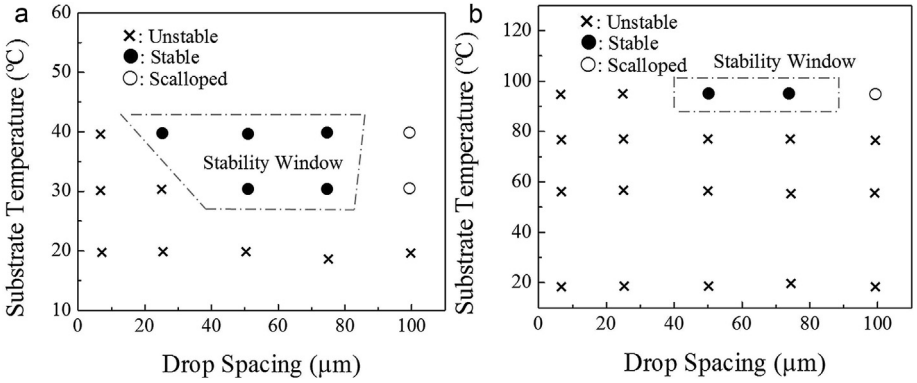

Fig. 4. Effect of substrate temperature on the conditions for printing stable YAG sol lines using (a) YWP inks and (b) YWEP inks.

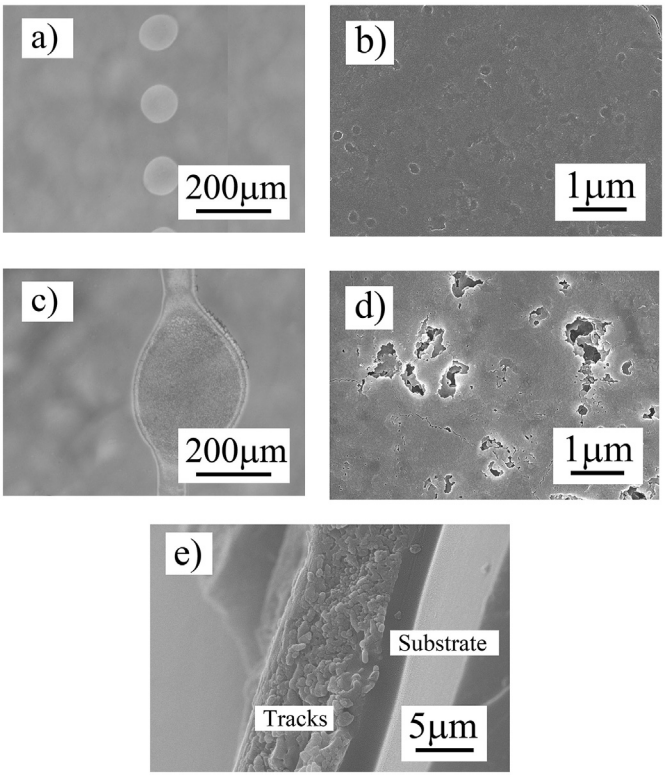

Fig. 7. Optical microscopy (a and c) images and the SEM micrographs (b, d and e) of the surface and cross-section of lines printed at 25 °C using YWP ink and then fired at 1200 °C for 1 h. a) optical microscopy image of isolated drops with ~120 nm thickness; b) SEM micrograph of the surface of a); c) optical microscopy image of bulges with ~300 nm thickness; d), SEM micrograph of the surface of c) in the bulge area; and e) SEM micrograph of cross-section of a bulge.

$$Z = \frac{\sqrt{\gamma \rho a}}{\eta} \quad (1)$$

wherein η is the viscosity, γ is the surface tension, ρ is the density and a is the diameter of drops. In general, inks are printable if $1 < Z < 10$ [13]. Ascan be seen from Table 2, the Z values for all inks are in the printable regime.

3.2. Stability of the printed line

The optical images of the printed lines using YWP ink are shown in Fig. 1. We did not observe any lines with straight edges (*i.e.* stable lines) for drop spacing p from 5 to 200 μm. When the drop spacing was small (*i.e.* $p = 5–50$ μm), bugles were always formed. When p was between 100 and 200 μm, only isolated or coalesced drops were observed.

When substrates were heated to temperatures above room temperature during printing, stable lines were obtained using the YWP ink, as shown in Fig. 2. As shown in Fig. 2 a, at 57 °C, the line morphology presenting bulges was very similar to the one obtained at room temperature for the same drop spacing (*e.g.*, $p = 50$ μm, Fig. 1 c). Upon increasing the substrate temperature to 95 °C, stable lines without bulges were observed as shown in Fig. 2 b). For a drop spacing of $p = 100$ μm, when the substrate temperature was increased to 76 °C, lines with 'scalloped' edges, also called 'scalloped lines', was observed (Fig. 2 c), rather than separated drops obtained at room temperature. Scalloped lines were also observed at 95 °C (Fig. 2 d), similar to the situation at 76 °C with the same drop spacing.

The effect of the p parameter on line stability was investigated using YWEP ink (Fig. 3). Again, when substrate temperature was 25 °C, bulges were observed for small drop spacing (*i.e.*, $p = 5–50$ μm) and separated droplets were observed when the drop spacing was 100 μm. Once substrate temperature was increased to 40 °C, bulges were still observed for $p = 5$ μm, but lines were stable for $p = 50$ μm and $p = 100$ μm. When drop spacing set at 100 μm, scalloped lines were observed. The edges of the lines for $p = 100$ μm were slightly scalloped, indicating that the spacing was too large to form lines with straight edges [17].

One of the most relevant challenges for printing YAG lines using sol-gel ink is line stability. Considerable effort has been made to understand line stability during inkjet printing. Davis concluded that in order to form stable line, the contact lines of a printed line must be fixed on the substrate in order to form stable lines when the nominal contact angle is less than 90° [18]. The boundary condition of fixed contact lines assumes that drops must be pinned on the substrate. However, this boundary condition is too strong and is hard to be realized in many practical printing situations. A weaker boundary condition was proposed by Duineveld [17], where contact lines can move forward but may not move backward. In other words, drops are only partially pinned on the substrate. Inks that have finite advancing contact angle but zero receding contact angle on substrates can satisfy this requirement, such as powder-based inks [9,20]. In this work, our sol-gel inks did not meet these requirements. The measured receding contact angles were not zero, as shown in Table 2. The drops were not pinned onto the substrates and thus we observed unstable lines at 25 °C. These observations match previous studies [17–19]. However, when the substrates were slightly heated, we observed new stable printing condition windows that are shown in Fig. 4. From Fig. 4, we can conclude that in general, increasing substrate temperature helps stabilize the printing tracks.

3.3. Sintering of the printed lines

Fully-dried YAG:Er^{3+} lines printed from all inks had uniform morphology without cracks or pores, as shown in Fig. 5. After firing at 1200 °C for 1 h, the printed lines from the YW ink presented severe buckling and cracking, as shown in Fig. 6. The addition of

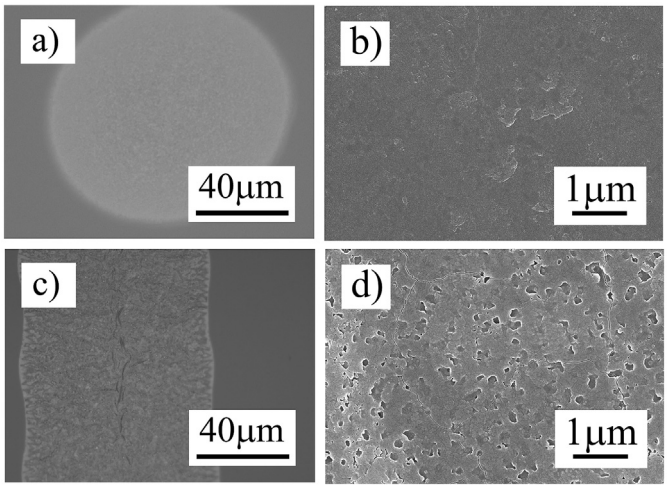

Fig. 8. Optical microscopy images (a and c) and the SEM micrographs (b and d) of the surface of lines printed at 95 °C using the YWP ink and then fired at 1200 °C for 1 h. a) optical microscopy image of one isolated drop with ~120 nm thickness; b) SEM micrograph of the surface of a); c) optical microscopy image of lines with ~200 nm thickness; d) SEM micrograph of the surface of c).

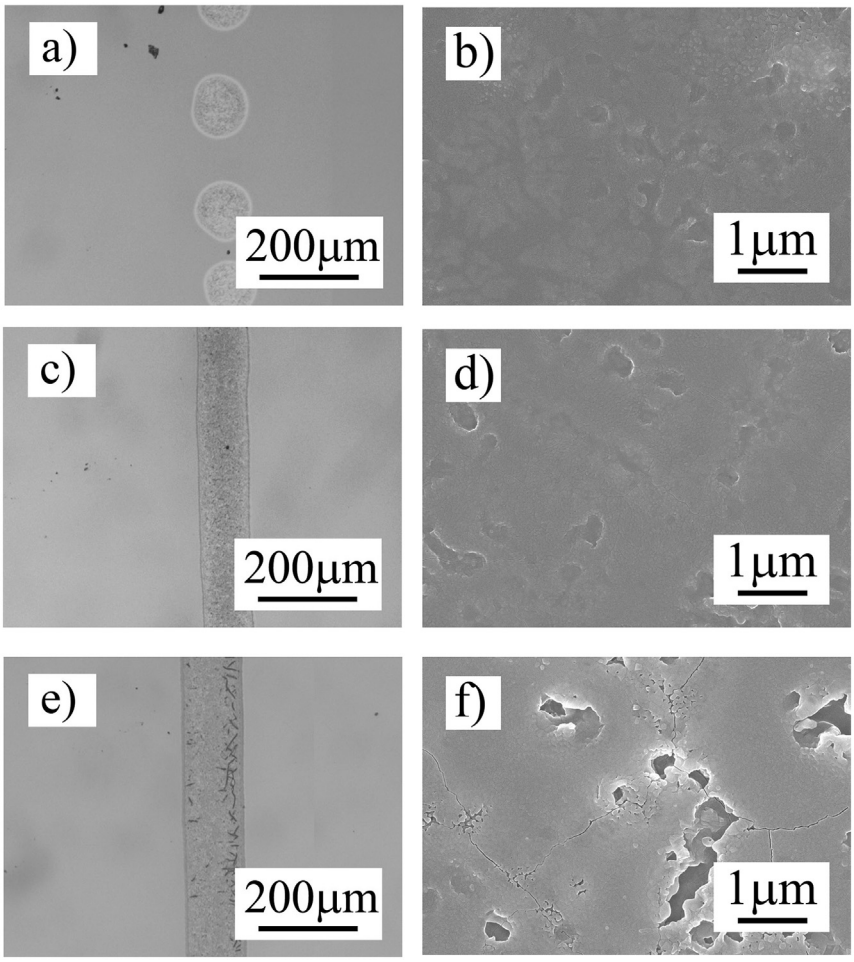

Fig. 9. Optical microscopy images (a, c, and e) and the SEM micrographs (b, d, and f) of the surface of lines printed at 40 °C using YEWP ink and then fired at 1200 °C for 1 h. a) optical microscopy image of isolated drops with ~120 nm thickness; b) SEM image of the surface of a); c) optical microscopy image of lines with ~200 nm thickness; d) SEM image of the surface of c); e) optical microscopy image of lines with ~300 nm thickness; f) SEM micrograph of the surface of e).

PVP to the YWP ink yielded crack- and buckle-free printed lines, as revealed by optical microscopy (Fig. 7 a and c). The isolated drops with ~120 nm thickness appeared dense and pore-free (Fig. 7 b). However, some pores were observed on the surface of the bulge (Fig. 7 d). The surface morphology of lines printed using YWP ink with substrate at 95 °C was different from that of the other lines: some wrinkles were found on the surface of the lines as shown in Fig. 8 c). The surface without wrinkles was still dense and pore-free, as shown in Fig. 8a) and b), but many pores were observed on the wrinkled surface (Fig. 8 d).

Optical images and SEM micrographs of lines printed using YWEP ink at 40 °C are shown in Fig. 9. No buckles were observed in tracks printed using YWEP ink, as shown in Fig. 9c) and d). The increase of the thickness of tracks led to the appearance of pores and cracks. For example, when the thickness of the sintered deposition was ~120 nm, no cracks were observed as shown in Fig. 9a) and b). Dense morphology was observed for lines with thickness ~200 nm, as shown in Fig. 9c) and d). Cracks were observed under optical microscopy when the track thickness was greater than ~300 nm, as shown in Fig. 9e) and f).

3.4. The relation between line stability, line thickness, cracking and pores

Dense and crack-free lines are desired for inkjet-printed

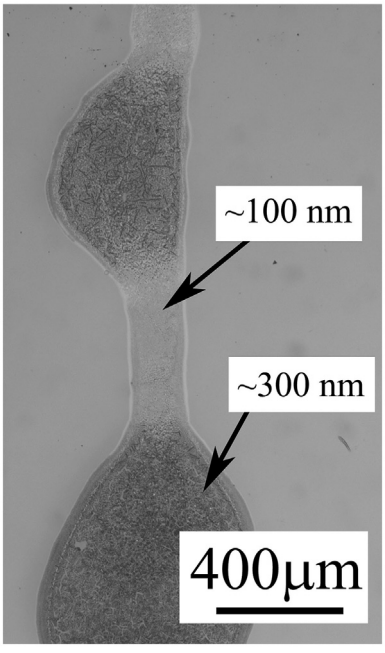

Fig. 10. Optical microscopy image of an unstable track printed using YWEP ink. Substrate was at room temperature and drop spacing = 5 μm.

Table 3
Thickness of printed lines using YWP and YWEP inks at different position.

Position within lines	Thickness of the lines using YWP ink	Thickness of the lines using YWEP ink
At the bulges	~300 nm	~200–300 nm
At the bridges between bulges	~90–100 nm	~90–100 nm
Stable lines	For drop spacing of 50 μm: ~200 nm For drop spacing of 25 μm: ~300 nm	

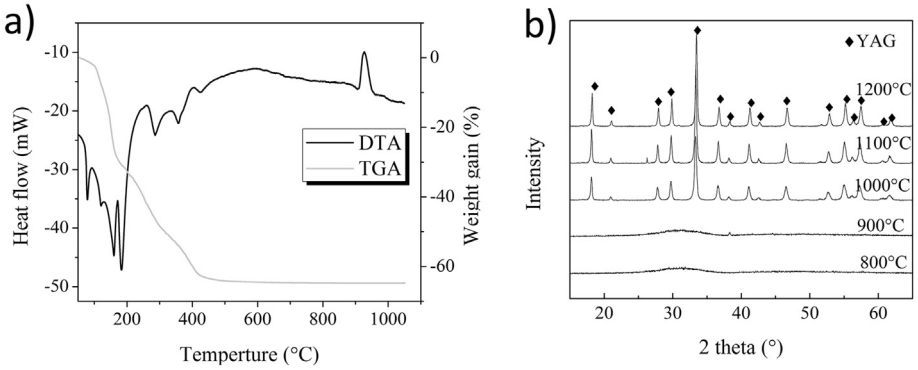

Fig. 11. a) DTA and TGA traces of YAG sol-gel powder, and b) XRD diffractograms of YAG after firing at different temperatures.

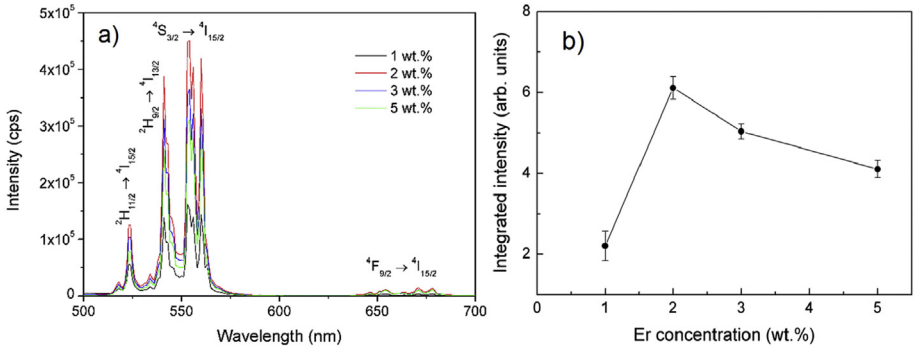

Fig. 12. a) PL spectra of YAG:Er powders with different Er concentrations heat treated at 1200 °C. b) Integrated PL intensity as a function of Er concentration.

scintillating and other functional devices. Generally, the critical thickness, above which the sol-gel deposition will have cracks, is less than 100 nm [20]. In this work, the lines printed using YW ink showed severe cracking in regions where thickness is ~120 nm after firing, as shown in Fig. 5. PVP is a stress relaxation agent that can greatly increase the critical thickness of ceramic layers prepared by sol-gel deposition [20,21]. Since PVP is not present during sintering, the most likely reason for this observation is that the incipient cracks are formed during drying and these cracks grow during sintering. PVP prevents the formation of incipient cracks. We obtained crack-free drops with thickness ~120 nm after the addition of PVP to the inks, as shown in Fig. 6 a and Fig 8 a.

Surface wrinkling was only observed on the lines printed using YWP ink at 95 °C. This phenomenon has been observed in the drying process of polymer solutions [22–24]. The surface wrinkling is caused by the failure of a structural member of a system subjected to compressive stress, and in this case can be triggered by the mechanical instability in a hard shell-soft core structure [23]. It is speculated that at 95 °C the evaporation rate was so high that the outer layer of the lines became hard while the core remained soft. The pores observed on the buckled surface were possibly caused by gas effusion during the fast solvent evaporation. Consequently, it is not possible to have stable, dense and crack-free lines printed using

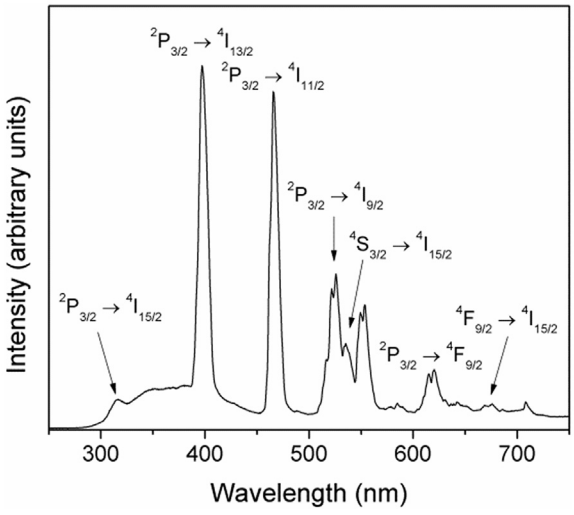

Fig. 13. Radioluminescence spectrum of YAG:Er powders activated with 2 wt% heat treated at 1200 °C. The electronic transitions of the main emission lines are shown.

YWP ink. On the other hand, lines printed using YWEP ink can be stable at 40 °C without buckling.

Line stability also influences the thickness of the printed lines. For unstable lines, the thickness at the bulges was much greater than that at the bridges between them. A typical example is shown in Fig. 10, where the thickness at the bulges was about three times thicker than that at the bridges. For stable lines, the thickness was uniform. Table 3 shows thickness of printed lines using YWP and YWEP inks at different positions. The line thickness at the bulges was about ~200–300 nm. The thickness of the bridges between bulges was ~100 nm. When lines are stable, thickness depended on drop spacing, with lower drop spacing resulting in larger thickness, as summarized in Table 3.

3.5. Crystallinity

DTA and TGA curves are shown in Fig. 11 a). The endothermic peaks from 100 to 300 °C in the DTA curve correspond to the evaporation of absorbed solvents and decomposition of low molecular weight polymers. The major decomposition occurred within 300–450 °C and was due to the elimination of alkoxy and nitrate [25]. The exothermic peak at 920 °C was attributed to the crystallization of YAG. The DTA results were consistent with the XRD results shown in Fig. 11 b). The powder remained amorphous for firing temperatures below 1000 °C and showed crystalline YAG phase for temperatures above 1000 °C. No intermediate phases, such as such as $YAlO_3$ (YAP) or $Y_4Al_2O_9$ (YAM) were observed from 800 °C to 1200 °C. These impurity phases are undesirable for efficient luminescence and should be avoided [26].

3.6. Luminescence

The application of direct inkjet printing to fabricate miniaturized scintillating devices based on YAG requires luminescence activation, commonly with a rare earth. In order to demonstrate that rare earth based luminescent materials can be fabricated by this method, YAG was activated with Er. Further, in order to evaluate how materials prepared by this method respond to the variation of the activator concentration, YAG was prepared with different amounts of the activator.

Luminescence was characterized by means of photoluminescence and radioluminescence measurements. These measurements revealed well-defined emission lines corresponding to Er^{3+} 4*f*-4*f* transitions. Photoluminescence spectra of YAG:Er^{3+} powder heat-treated at 1200 °C for 1 h obtained under the same experimental conditions are shown in Fig. 12a) for different Er doping concentrations. A series of well-defined emission lines from 510 to 580 nm originated in the $^2H_{11/2} \rightarrow {}^4I_{15/2}$, $^4S_{3/2} \rightarrow {}^4I_{15/2}$, and $^2H_{9/2} \rightarrow {}^4I_{13/2}$ transitions [27,28] were observed together with another series of weaker lines between 630 and 690 nm assigned to the $^4F_{9/2} \rightarrow {}^4I_{15/2}$ transition [27]. The overall photoluminescence intensity of the green emission was estimated by integrating the intensity from 500 to 600 nm. It was found that 2 wt% Er optimized photoluminescence, with further increase in the Er concentration resulting in intensity decrease due to concentration quenching [29] (Fig. 12b). Scintillation was evaluated under X-ray excitation for this particular composition (Fig. 13). The radioluminescence spectrum was dominated by transitions $^2P_{3/2} \rightarrow {}^4I_{13/2}$ and $^2P_{3/2} \rightarrow {}^4I_{11/2}$ at 398 and 467 nm [29], respectively, that match the maximum detection efficiency of photomultiplier tubes. A broad band within about 300–450 nm was ascribed to the combined contribution of the $^2P_{3/2} \rightarrow {}^4I_{15/2}$ transition at 315 nm with the emission of several luminescent defects of the host. Emission at 295 nm is from the recombination of localized excitons at anti-site defects, emission at 260 nm from self-trapped excitons, at around 320–330 nm from Y_{Al} antisite defects, at around 400 nm from F^+ centers, and at around 460 nm from F centers [29–33]. Similar host emission has been reported previously in the literature [30–33]. These results confirmed that YAG produced by this method can be activated by rare earths to produce efficient luminescence.

4. Conclusions

The goal of this work was to achieve proof-of-concept of the fabrication of rare earth activated miniaturized scintillators based on YAG using the direct inkjet printing method as a first step toward fabricating scintillators with complex geometries. The direct inkjet printability of YAG:Er luminescent lines using sol-gel precursor was investigated for the first time. It was found that line stability was improved by heating the substrates. No stable lines were obtained at 25 °C and stable printing condition windows were obtained at 95 °C for water-based YAG inks and at 40 °C for the water-ethanol-based YAG ink. The line thickness was influenced by stability of the printed lines and the drop spacing. Bulges in unstable lines had larger thickness (~300 nm) and led to cracks and pores. Lines with thickness of ~200 nm printed using YWEP ink were dense and crack-free. YAG:Er^{3+} prepared by the proposed sol-gel method and fired at 1200 °C showed well-defined luminescence lines in the ultra-violet and visible regions, demonstrating the luminescence activation of the YAG host with rare earths.

Acknowledgements

This material is based upon work supported by the Department of Energy under grant DE-FE00012272, and the National Science Foundation under Grant No. 1207080.

References

[1] David W. Townsend, Positron emission tomography/computed tomography, in: Seminars in Nuclear Medicine, Vol. 38(No. 3), WB Saunders, 2008.
[2] C. Greskovich, S. Duclos, Ceramic scintillators, Annu. Rev. Mater. Sci. 27 (1) (1997) 69–88.
[3] A.S. Beddar, et al., A miniature "scintillator-fiberoptic-PMT" detector system for the dosimetry of small fields in stereotactic radiosurgery, Nucl. Sci. IEEE Trans. 48 (3) (2001) 924–928.
[4] A. Ohzu, M. Takase, M. Haruyama, N. Kurata, N. Kobayashi, M. Kureta, T. Nakamura, et al., Numerical evaluation of the light transport properties of alternative He-3 neutron detectors using ceramic scintillators, Nucl. Instrum. Methods Phys. Res. Sect. A Accel. Spectrom. Detect. Assoc. Equip. 798 (2015) 62–69.
[5] Kenichi Watanabe, Yuya Kawabata, Atsushi Yamazaki, Akira Uritani, Tetsuo Iguchi, Kentaro Fukuda, Takayuki Yanagida, Development of an optical fiber type detector using a Eu: LiCaAlF 6 scintillator for neutron monitoring in boron neutron capture therapy, Nucl. Instrum. Methods Phys. Res. Sect. A Accel. Spectrom. Detect. Assoc. Equip. 802 (2015) 1–4.
[6] Edita Garskaite, et al., Luminescent properties of rare earth (Er, Yb) doped yttrium aluminium garnet thin films and bulk samples synthesised by an aqueous sol–gel technique, J. Eur. Ceram. Soc. 30 (7) (2010) 1707–1715.
[7] Emanuel Sachs, et al., Three dimensional printing: rapid tooling and prototypes directly from a CAD model, J. Eng. Industry 114 (4) (1992) 481–488.
[8] Julian RG. Evans, Mohan J. Edirisinghe, Jin-Hua Song, Direct ink-jet printing of vertical walls, J. Am. Ceram. Soc. 85 (8) (2002) 2113–2115.
[9] Rui Dou, et al., Ink-Jet printing of zirconia: coffee staining and line stability, J. Am. Ceram. Soc. 94 (11) (2011) 3787–3792.
[10] Yeonjun Oh, et al., Inkjet-printing of TiO_2 co-solvent ink: from uniform ink-droplet to TiO_2 photoelectrode for dye-sensitized solar cells, J. Electrochem. Soc. 159 (1) (2011) B34–B38.
[11] Nuno Reis, Christopher Ainsley, Brian Derby, Viscosity and acoustic behavior of ceramic suspensions optimized for phase-change ink-jet printing, J. Am. Ceram. Soc. 88 (4) (2005) 802–808.
[12] Tianming Wang, Brian Derby, Ink-Jet printing and sintering of PZT, J. Am. Ceram. Soc. 88 (8) (2005) 2053–2058.
[13] Kitty AM. Seerden, et al., Ink-jet printing of wax-based alumina suspensions, J. Am. Ceram. Soc. 84 (11) (2001) 2514–2520.
[14] B. Cappi, et al., Direct inkjet printing of Si_3N_4: characterization of ink, green bodies and microstructure, J. Eur. Ceram. Soc. 28 (13) (2008) 2625–2628.
[15] Brian Derby, Additive manufacture of ceramics components by inkjet printing, Engineering 1 (1) (2015) 113–123.

[16] A. Atkinson, et al., Continuous ink-jet printing using sol-gel “ceramic” inks, J. Sol-Gel Sci. Technol. 8 (1–3) (1997) 1093–1097. Duineveld, Paul C. “The stability of ink-jet printed lines of liquid with zero receding contact angle on a homogeneous substrate.” Journal of fluid mechanics 477(2003): 175–200.
[17] Stephen H. Davis, Moving contact lines and rivulet instabilities. Part 1. The static rivulet, J. Fluid Mech. 98 (2) (1980) 225–242.
[18] Stefano Schiaffino, Ain A. Sonin, Formation and stability of liquid and molten beads on a solid surface, J. Fluid Mech. 343 (1997) 95–110.
[19] Jonathan Stringer, Brian Derby, Formation and stability of lines produced by inkjet printing, Langmuir 26 (12) (2010) 10365–10372.
[20] Zhaoxi Chen, et al., The effect of polymer additives on the critical thicknesses of mullite thin films obtained from the monophasic sol–gel precursors, J. Sol-Gel Sci. Technol. (2016) 1–12.
[21] Hiromitsu Kozuka, et al., Crack-free, thick ceramic coating films via non-repetitive dip-coating using polyvinylpyrrolidone as stress-relaxing agent, J. Sol-Gel Sci. Technol. 19 (1–3) (2000) 205–209.
[22] K. Sefiane, L. Tadrist, M. Douglas, Experimental study of evaporating water–ethanol mixture sessile drop: influence of concentration, Int. J. Heat Mass Transf. 46 (23) (2003) 4527–4534.
[23] Lifeng Wang, et al., Wrinkled surface topographies of electrospun polymer fibers, Appl. Phys. Lett. 94 (15) (2009) 151916.
[24] Troy R. Hendricks, Ilsoon Lee, Wrinkle-free nanomechanical film: control and prevention of polymer film buckling, Nano Lett. 7 (2) (2007) 372–379.
[25] Michael Veith, et al., Low temperature synthesis of nanocrystalline $Y_3Al_5O_{12}$ (YAG) and Ce-doped $Y_3Al_5O_{12}$ via different sol–gel methods, J. Mater. Chem. 9 (12) (1999) 3069–3079.
[26] Guodong Xia, et al., Structural and optical properties of YAG: Ce 3+ phosphors by sol–gel combustion method, J. Cryst. Growth 279 (3) (2005) 357–362.
[27] John B. Gruber, et al., Energy levels and correlation crystal-field effects in Er 3+-doped garnets, Phys. Rev. B 48 (21) (1993) 15561.
[28] Y. Yu, et al., Concentration effects of Er ion in YAG: Er laser crystals, J. Alloys Compd. 302 (2000) 204–208.
[29] Yu Zorenko, et al., Luminescent properties and energy transfer processes in YAG: Er single crystalline films, J. Luminescence 154 (2014) 198–203.
[30] Yu Zorenko, et al., Exciton and antisite defect-related luminescence in Lu3Al5O12 and Y3Al5O12 garnets, Phys. Status Solidi (b) 244 (2007) 2180–2189.
[31] Y. Zorenko, et al., Luminescence of F+ and F centers in Al2O3-Y2O3 oxide compounds, in: IOP Conference Series: Materials Science and Engineering, Vol. 15(No. 1), IOP Publishing, 2010.
[32] Y. Zorenko, et al., Luminescence of excitons and antisite defects in the phosphors based on garnet compounds, Rad. Meas. 38 (2004) 677.
[33] Y. Zorenko, et al., Single crystalline film scintillators based on Ce- and Pr-doped aluminium garnets, Rad. Meas. 42 (2007) 521.